Ultrasonics Sonochemistry 85 (2022) 105990

Contents lists available at ScienceDirect

Ultrasonics Sonochemistry

journal homepage: www.elsevier.com/locate/ultson

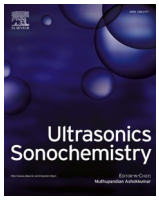

In-depth analysis of ultrasonic-induced geological pore re-structures

Leng Tian [a,b], Hengli Wang [a,b], Tao Wu [a,b], Haien Yang [c], Shuwen Xu [d], Xiaolong Chai [a,b], Kaiqiang Zhang [e,*]

[a] State Key Laboratory of Petroleum Resources and Prospecting in China University of Petroleum Beijing 102249, PR China
[b] College of Petroleum Engineering, China University of Petroleum, Beijing 102249, PR China
[c] Oil and Gas Technology Research Institute of Petro China Changqing Oilfield Company, Xi'an 710018, PR China
[d] CNPC Logging Co., Ltd. North China Branch, Renqiu 062550, PR China
[e] Institute of Energy, Peking University, Beijing 100871, PR China

ARTICLE INFO

Keywords:
Ultrasonics
Pore restructures
In-situ core
Analytical instrument
Characterization and interpretation

ABSTRACT

Understanding and manipulating geological pore structures is of paramount importance for geo-energy productions and underground energy storages in porous media. Nevertheless, research emphases for long time have been focused on understanding the pore configurations, while few work conducted to modify and restructure the porous media. This study deploys ultrasonic treatments on typical geological in-situ core samples, with follow-up processes of high-pressure mercury injections and nitrogen adsorptions and interpretations from nuclear magnetic resonance and x-ray diffraction. The core permeability and porosity are found to increase by 8.3 mD, from 4.1 to 12.4 mD, and by 0.95%, from 14.03% to 14.98%, respectively. Meanwhile, the number and size of the micro- and mesopore are increased with progressing of ultrasonic treatment, while those of the macropore decrease, which finally increase the permeability and porosity. The increase of micro- and mesopore number, from x-ray diffraction results, is attributed to the migration and precipitation of clay minerals caused through ultrasonic wave. The relocation of clay minerals also helps to improve the pore-throat connectivity and modify the micro-scale heterogeneity. Basically, this study reveals the characterizations of geological pore reconfigurations post-ultrasonic treatments and interprets the associated mechanisms, which provides guidance to manipulate the geological pores and be of benefit for further porous media use in science and engineering.

1. Introduction

Geological porous media, particularly those with complex structures and low-permeability, attract increasing attentions due to the geo-energy productions and geological site usages for energy storages [1–3]. It is the key to the development of low permeability reservoirs that how to established an effective displacement pressure system between injection and production wells [4–6]. Unfortunately, the rapid pressure drop caused by the increase of seepage resistance near vertical wellbore is disadvantage to the establishment of effective inter-well displacement pressure system [7,8]. Robert et al. used the universal material balance method to describe changes in reservoir pressure during horizontal well production and got similar conclusions [9]. High-speed non-Dacry flow near well region aggravates the pressure drop [10]. Additionally, permeability decline due to reservoir blockage around wellbore during drilling and production, which in turn leads to a rapid decrease in near-wellbore pressure [11–13]. In order to solve this problem, ultrasonic technology is used to treatment formation trying to remove blockage near wellbore. It is found that the reservoir blockage is relieved and the permeability is increased after treatment, which effectively delays the pressure drop in the near-well zone [14–16]. Therefore, it is of a practical and fundamental importance to study the change of pore structure of reservoir treated by ultrasonic for the analysis of near-wellbore pressure drop.

Compared with the traditional reservoir fracturing technology based on chemical or physical methods, the characteristics of good economy, friendly environment and long effective time promotes acoustic wide application in reservoir development [17–21]. From 1950 s till present, researchers have perceived that ultrasound can reduce crude oil viscosity, reduce oil–water interfacial tension, enhance capillary imbibition, and increase reservoir permeability after a large number of studies on the mechanism of ultrasonic enhanced oil recovery, they also believe that the power, frequency and handing time of ultrasound will affect the efficiency of ultrasound in enhancing oil recovery [22–28]. Ultrasonic

* Corresponding author.
E-mail address: kaiqiang.zhang@pku.edu.cn (K. Zhang).

https://doi.org/10.1016/j.ultsonch.2022.105990
Received 14 January 2022; Received in revised form 15 March 2022; Accepted 23 March 2022
Available online 24 March 2022

oil recovery technology is widely used to be treated the blocking near well oil layers caused by deposition of particles in porous media, the purpose of increasing the crude oil production, water injection rate and oil recovery is achieved [29,30]. Daily production from wells in western Siberia increased by an average of 5.2 tons per day after ultrasonic stimulation of the near wellbore region [31]. The reason is that the high frequency vibration of ultrasonic wave drives the pore walls to vibrate and the fluid is forced through pores [32]. Simultaneously, the porosity and permeability of near well region are increased due to asphaltene and paraffin deposits were cleaned from pores, and well production increased [33].

Obviously, the pore structure near the well zone has changed after ultrasonic treatment. Ali investigated the pore structure change of sandstone after ultrasonic wave treatment through scanning electron microscope images and petrography, the permeability of sandstone was increased due to exfoliation of rock particles and formation of micro-fractures after treatment, but not absolutely, as exfoliated particles may also block the pore throat and cause permeability reduction [34]. Li analyzed the EOR mechanism of ultrasonic waves in the low-permeability reservoir by scanning electron microscopy and fourier transform infrared spectroscopy and concluded that ultrasonic wave can alter the micromorphology of low-permeability cores and improve the pore connectivity [35]. Li analyzed the results of nitrogen adsorption experiment and found that ultrasonic waves not only accelerated the gas desorption rate, but also increased the pore size and specific surface area of shale [36]. Due to the lack of systematic research on the effect of ultrasonic wave on sandstone pore structure, the relevant research methods and theories of ultrasonic treatment of coal seam can provide some inspiration for our research. The change of pore number and size and the development of coal fractures with ultrasonic excitation were determined by using nuclear magnetic resonance, thermal imaging and P-wave measurement system by Tang (2016) [37]. Shi investigation the change of pore type and diameter was analysed by using N_2 gas adsorption and summarized that the pore type of coal was not changed after ultrasonic treatment but porosity was increased [38]. Liu and Sun found by scanning electron microscopy that ultrasound could further expand existing pores and cracks in coal and remove organic matter and minerals on its surface [39,40]. Li coupled the temperature, pressure, and seepage parameters of the coalbed methane reservoir and built a seepage model under the action of ultrasonic waves for verifies that uses ultrasonic waves to improve the seepage characteristics of coalbed methane reservoir [41]. In addition, ultrasound is also used to increase the specific surface area and porosity of activated carbon and sludge [42,43]. So far, no attempts have been made to quantify the effect of ultrasonic on pore and throat structure changes in sandstone by combining nuclear magnetic resonance (NMR), high pressure mercury injection (HPMI), low-temperature nitrogen adsorption (LTNA) and X-ray diffraction (XRD).

In this paper, the changes of pore and throat structure after ultrasonic waves treatment for different time were comprehensively characterized by combined with HPMI, NMR, LTNA and XRD. Specifically, including changes in the number of micro to nanoscale pores, throat size, pore-throat connectivity and the variation of microscopic heterogeneity. In addition, the core permeability and porosity changes with the ultrasonic treatment time are also monitored. The rule of the pore structure change in the near well area was discovered by this study would provide reference and support for the optimization of production pressure difference and injection-production parameters of ultrasonic oil recovery, which is conducive to promoting application of ultrasonic oil recovery technology and improving recovery efficiency of low permeability reservoirs.

2. Experimental

2.1. Materials

A core sample with length of 11.6 cm and width of 2.5 cm is collected from the Upper Triassic Yanchang formation of the Chang 6 sandstone reservoir in the Ordos Basin, China. The long core is divided into five sections from left to right, they will be used for HPMI, NMR, LTNA and XRD test, the size of the cores is shown in Fig. 1. Because the residual oil in pores of samples will be affected the accuracy of the experiment, the organic in samples must be eluted by a mixture of dichloromethane and methanol with a volume ratio of 9 to 1. The synthetic brine was prepared by using distilled water with the salinity of 22070 mg/L (i.e., 7990 mg/L KCl, 1090 mg/L $CaCl_2$, 2410 mg/L $MgCl_2$, 8620 mg/L NaCl, and 1960 mg/L $NaHCO_3$). Such prepared synthetic brine was used as reservoir brine to eliminate the influence of the water sensitivity according to the formation water salinity and ion types of Chang 6 reservoir.

2.2. Setup

Fig. 2 shows the structure of Soxhlet extractor (SGLT-6, Shanghai Luwin Scientific Instrument Co., LTD, China), which is mainly composed of round bottom flask, absorbent cotton, extraction tank and condensor. The round bottom flask can hold up to 1.5L of the extraction solvent, from which it is vaporized into the extraction tank. Running water in the condenser cools the vaporized extraction solvent into a liquid and drops it onto the core in the extraction tank.

The ultrasonic cleaning can provide ultrasonic waves with fixed frequency (28 kHz) and power (120 W) for the experiment. In order to avoid the experimental error caused by water sensitivity effect, the machine conducts ultrasonic waves to the rock with brine as the medium, and the temperature adjustment range is from surrounding temperature to 373.2 K. The running time of the machine can be set at most 3 h at a time, but it can be set continuously, so the time is free.

The experimental device for gas permeability measurement is self-assembled, which is mainly composed of nitrogen cylinder with pressure regulator, core holder, hand pump and gas metering device. The nitrogen cylinder provides displacement pressures of 0.01 MPa-10 MPa for permeability tests, and the gas metering device attached to the outlet side measures the volume of gas flowing per unit time when the high-pressure gas passes through the core holder. Of course, the hand pump provides the core gripper with a constant confining pressure of 2 MPa

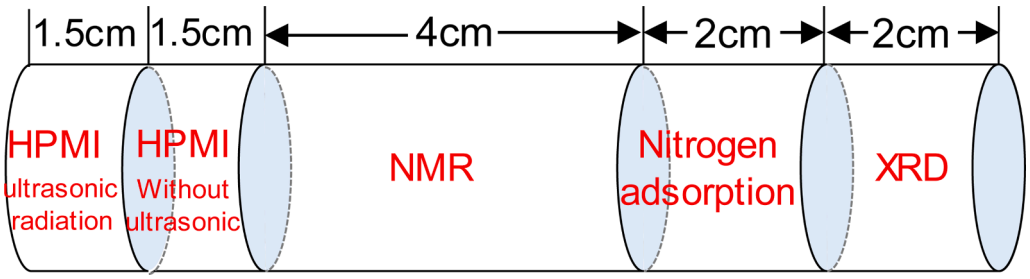

Fig. 1. The cutting position of a core sample.

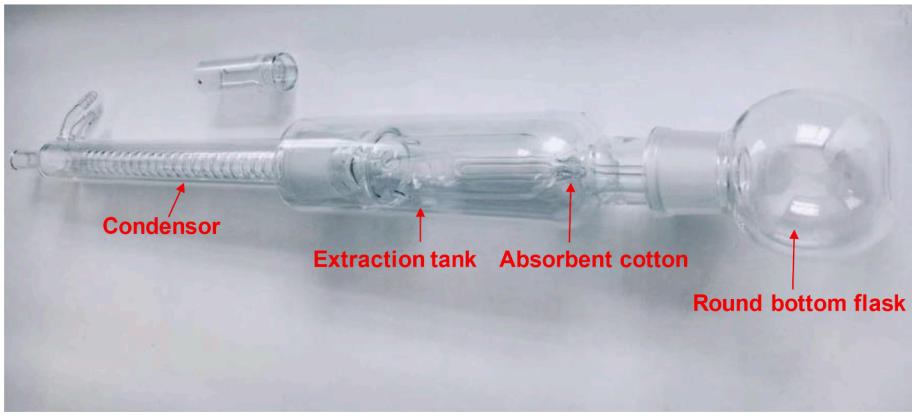

Fig. 2. Structure and composition of Soxhlet extractor.

above the inlet pressure to prevent gas from passing through the gap between the core and the gripper in this process.

The instrument model used in this HPMI experiment is Autopore IV 9520 automatic mercury porosimeter manufactured by American Instruments. The minimum pore size detected was 0.003 μm when the mercury injection pressure reaches the maximum allowable pressure of 413 MPa, and the measurement accuracy is 0.001 MPa. The mercury injection process used a staged pressure boost, and the cumulative mercury injection saturation under a certain pressure was recorded after the pressure reached stability. The pore-throat radii under different pressures can be obtained according to the Washburn equation.

NMR pulsar (come from Oxford instruments, UK) is used to detect the transverse relaxation time (T_2) spectrum, including a magnet, a RF emitter and a data acquisition unit. The radio frequency is distributed in a range of 1–30 MHz with a control precision of 0.1 MHz. Besides, the echo time is set to be 0.12 ms, waiting time is 1.125 s for measurement, and the scanning number is 64.

The experimental equipment for LTNA is QUADRASORB SI specific surface analyzer produced by Anton Paar Company in the United States, which can be used to measurement any specific surface (0.0005 m^2/g) and pore size (0.35 nm-500 nm) at the same time by an independent analysis station.

The polycrystalline diffractometer (Empyrean, Malvern Panaco, Netherlands) used for XRD diffraction testing has a minimum step angle of 0.0001° and repeatability of 0.0001, the angle deviation of less than ± 0.01°. The core needs to be ground into a 200 mesh powder in a dry environment.

2.3. Procedure

In this section, a detailed description of experiment procedure will be provided as follows:

Step 1: In this paper, the organic content in the core was cleaned by Soxhlet apparatus. The core was placed in the extraction tank of the Soxhlet instrument, and fill the flask with 1 L of a mixture of dichloromethane and methanol with a volume ratio of 9 to 1. Vaseline was applied to each port to seal, and tap water was supplied to the condensate tube to cool and turn on the heating unit. The extraction solvent in the flask is vaporized as solvent vapor with heat, and then drops into the extraction tank through the condensing tube to extract the organic matter in the rock. With the accumulation of solvent in the extraction tank, the solvent flows into the flask through the siphon when the liquid level reaches a certain height. This process is repeated until extraction is stopped after 20 days. The cores are removed and dried in constant temperature chamber for 10 h at 373.2 K.

Step 2: The core was cut into cylinders of the size required for the experimental in the sequence shown in Fig. 1 using a 6 Lapidary trimming saw (Kingsley North Inc., Norway, MI) with use of cooling water.

Step 3: The cut cores were dried in a constant temperature chamber at 370.2 K for 10 h, then weighed and cooled at room temperature for 10 h. Core diameter and length should be measured before gas permeability test. In order to avoid swelling of clay minerals in cores caused by water sensitivity, the cores were saturated with brine by vacuuming and pressurization. Specifically, the core is first placed in an intermediate container with a piston, and the vacuum pump is worked for 10 h to completely drain the air from the pistons. Then, the vacuum pump shut down and draws formation water into the piston under atmospheric pressure. When the container is filled with water, close the valve and push the piston to increase the pressure inside the piston to 19 MPa. 10 h later, the core was taken out and weighed to calculate porosity.

Step 4: The two samples with length of 1.5 cm on the left are used for HPMI experiment. One of the cores without ultrasonic treatment was first dried at 373.2 K in a constant temperature chamber for 10 h and cooled at room temperature for 10 h. The core was placed in a closed high-pressure chamber for vacuum test, and the injection pressure was stages increased, record the cumulative volume of mercury when the pressure reached stability. The mercury injection pressure can be converted to the pore-throat radius according to the Washburn equation. The other core needs to be treated continuously for 6 h in an ultrasonic cleaner filled with salt water before the HPMI experiment is carried out according to the above procedure.

Step 5: After step 3, the samples with a length of 4 cm were firstly tested by NMR, and then placed it in an ultrasonic cleaning machine filled with salt water for continuous stimulated for 2 h. According to the experimental steps described above, the core was dried, measured gas permeability, saturated water and NMR tested in sequence. The core was treated by ultrasonic for 2 h again, and this process was repeated until the core was treated for 6 h in total. Finally, the T_2 spectrum and permeability of the core without ultrasonic and treated for 2, 4 and 6 h by ultrasonic were obtained.

Step 6: After step 2, cores for LTNA experiments are dried and made into particles of 2 mm in diameter. Firstly, 2 g of particles was put into a closed glass tube for LTNA experiment without ultrasonic

effect. Then, the particles were treated in an ultrasonic cleaner for 2 h, and dried again for LTNA. Repeat this step until the cumulative ultrasonic treatment time reached 6 h. The specific surface area and number of nanopore of the core without ultrasonic and treated for 2,4 and 6 h by ultrasonic were obtained.

Step 7: Like the LTNA experiment, the core used for XRD test also needs to be dried and made into particles with a diameter of 2 mm. These particles are averaged to four parts, one of them directly ground to 200 mesh powder but other three parts should be treated by ultrasonic for 2, 4, and 6 h, drying and grinding to 200 mesh powder and tested for XRD. The mineral content of the core without ultrasonic and treated for 2,4 and 6 h by ultrasonic were obtained.

3. Result and discussion

3.1. Porosity and permeability

The relaxation signals when the pores of the core are fully saturated with single-phase water are all derived from the hydrogen atoms in the water molecules, consequently the core porosity can be obtained from the cumulative distribution curve of the T_2 spectrum. Fig. 3 is the porosity change of the sample after ultrasonic treatment by NMR monitoring. It shows that the initial porosity of the sample was 14.0% and which increased to 14.5% after 2 h of ultrasonic treatment, the porosity of ultrasonic treatment for 4 h and 6 h increased to 14.6% and 14.9%, respectively. Overall, porosity increases with the increase of ultrasonic treatment time, the increase in porosity varies in different stages of ultrasonic treatment due to the influence of core pore structure, cementation degree, mineral composition and other physical properties.

The change of permeability after ultrasonic treatment is shown in Fig. 4. Similar to the variation trend of porosity, permeability also increases with the increase of ultrasonic treatment time. The initial permeability of the sample was 4.6 mD, which increased to 10.4 mD after 2 h of ultrasonic radiation, the permeability increased to 11.9 mD and 12.4 mD after 4 h and 6 h of ultrasonic stimulate, respectively. Unfortunately, the increase amplitude of permeability decreases with the extend of processing time.

Obviously, the increase of porosity and permeability means that the seepage of fluid in the porous media will be easier. Especially, the increase of permeability significantly reduces the pressure loss in the near wellbore area of low permeability reservoirs and is of great significance to improve the production of oil wells. In this work, we will analyze and try to explain the reason of ultrasonic treatment increases core porosity and permeability in the following sections.

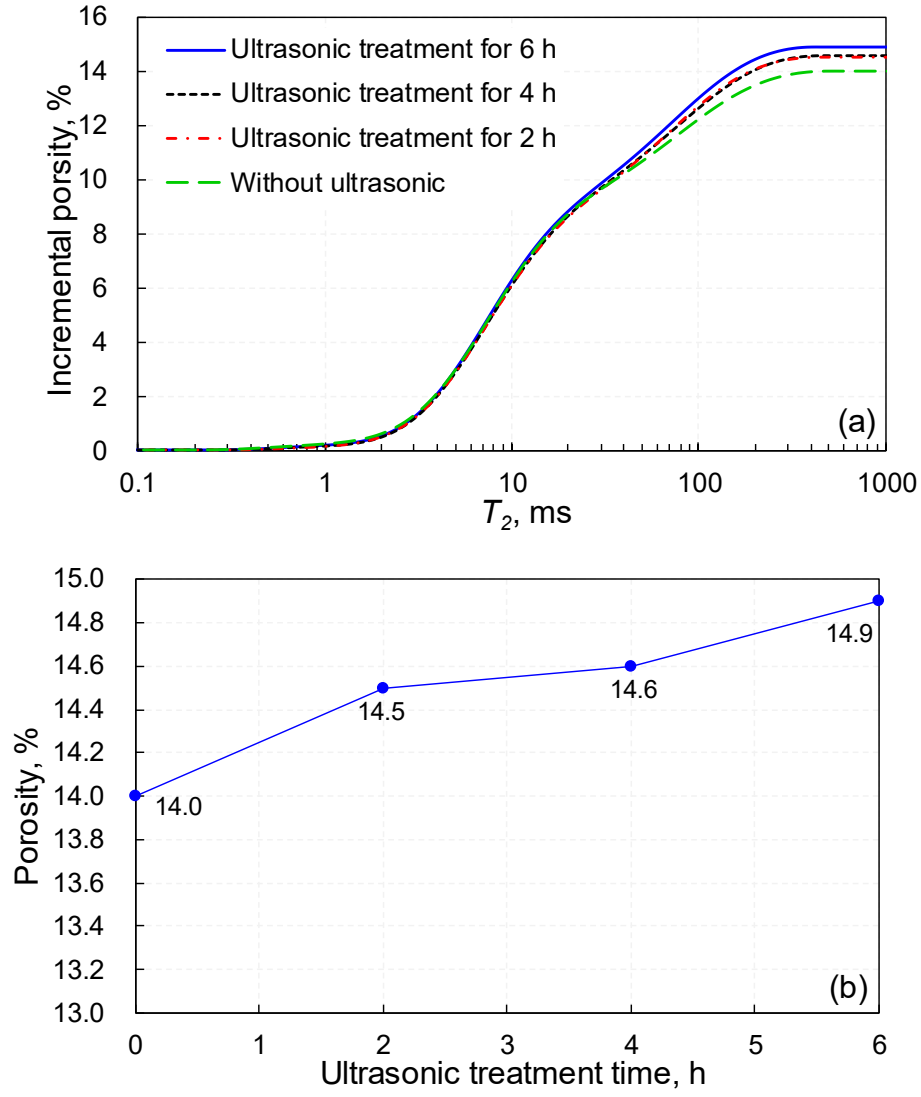

Fig. 3. Porosity of core after ultrasonic treatment: (a) Cumulative distribution of T_2 spectrum after ultrasonic treatment for different time and (b) changes of porosity after ultrasonic treatment for different time.

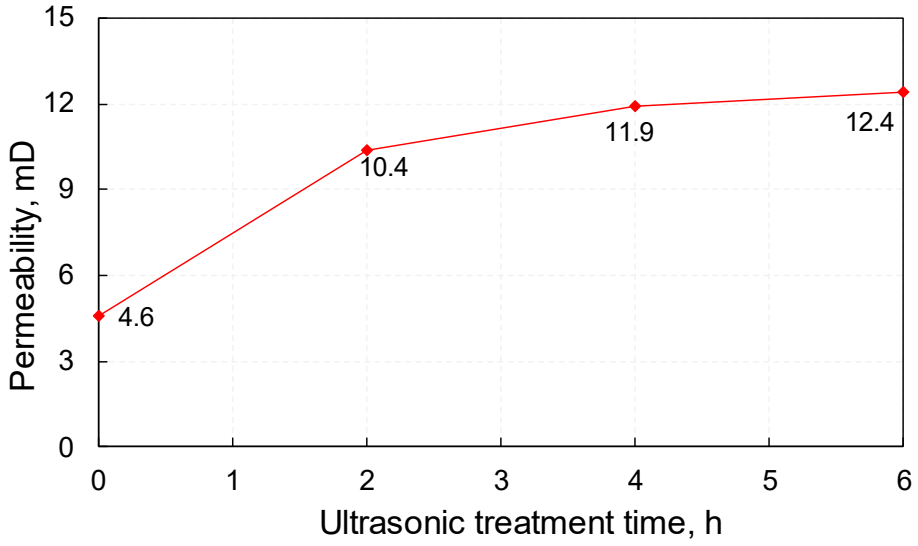

Fig. 4. The change of permeability after ultrasonic treatment for different time.

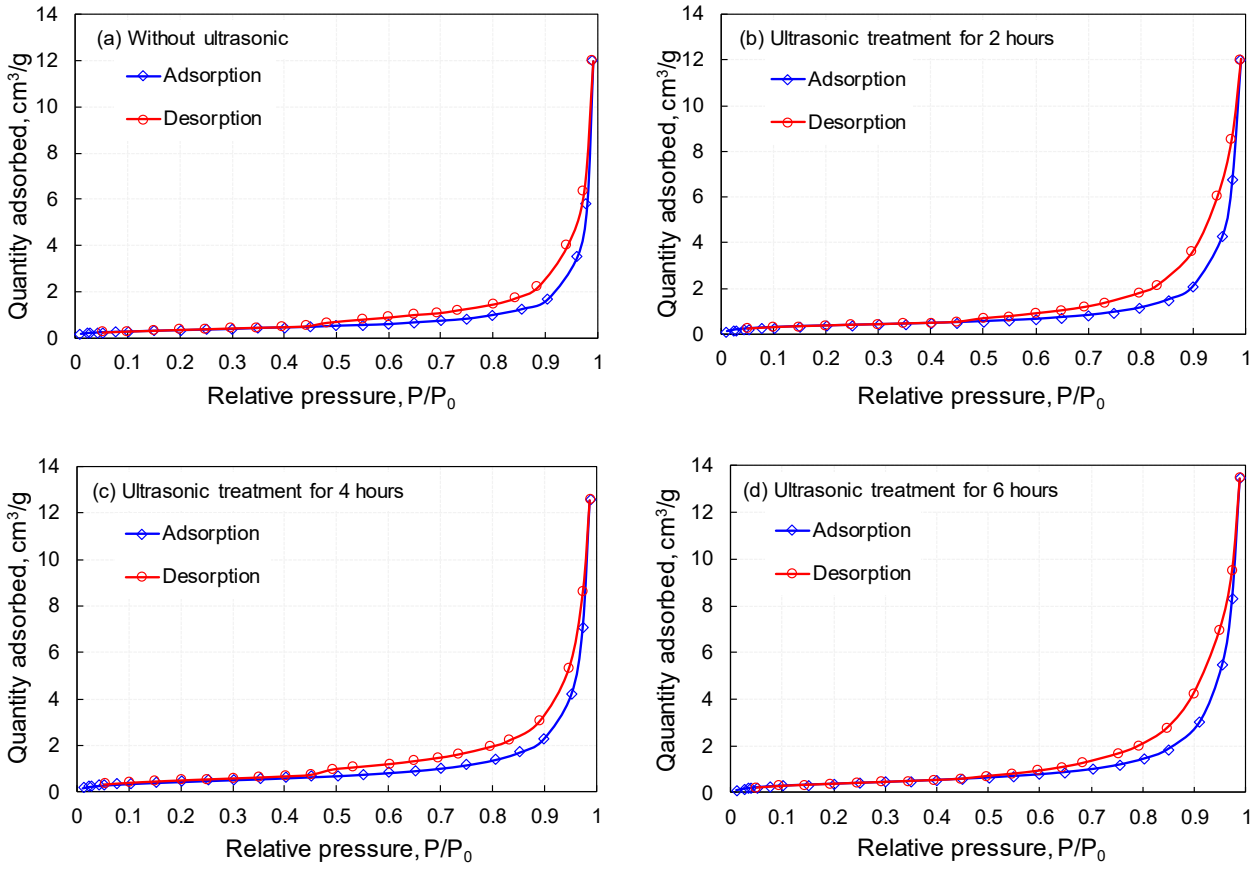

Fig. 5. Low-temperature nitrogen adsorption and desorption curves of cores treated with ultrasonic for different time.

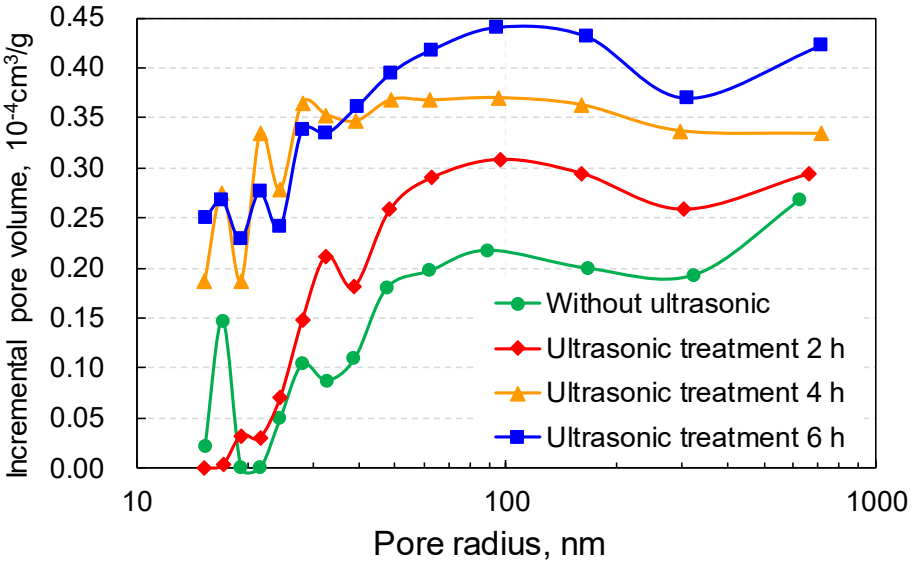

Fig. 6. Nanopores size distribution derived from LTNA.

3.2. Pore-throat size

Fig. 5 shows the Low-temperature nitrogen adsorption and desorption curves of cores treated with ultrasonic for different time. It can be seen from the figure that the early adsorption volume increased slowly until the adsorption amount increased rapidly after the relative pressure (P/P0) reached 0.85. The adsorption capacity increases rapidly and capillary condensation occurs as the relative pressure approximate to 1 indicates that the presence of large pore sizes in the core. The N_2 isotherm of adsorption and desorption are separated to form a hysteresis loop near the medium relative pressure ($P/P_0 = 0.45$). They all belong to the H3 type according to the International Union of Pure and Applied Chemistry (IUPAC) and the shape characteristics of the narrow lag ring, indicating the existence of a parallel plate-shaped slit nanopore in the rock [44]. Obviously, the shape of N_2 isotherm of adsorption and desorption did not change after ultrasonic treatment, indicating that ultrasonic radiation did not change pore type but pore size.

The Brunauer-Emmette-Teller and Barrett-Joynere-Halenda methods were used to calculate the specific surface area and pore volume, respectively [45,46]. The plot of dV/dlog(W) (V is pore volume, W is pore width) versus W is used to display the pore size distribution [47]. As shown in Fig. 6, the maximum pore size of nano-pores increased from 663.2 nm to 717.9 nm after ultrasonic treatment for 6 h, and the number of pores with the same size increased. The average radius of nanopores increased from 56.5 nm to 58.3 nm after ultrasonic treatment for 2 h, and increased to 75.9 nm after ultrasonic treatment for 6 h. In addition, the specific surface area increased with ultrasonic treatment time. The specific surface area of ultrasonic treatment for 2, 4 and 6 h were 2.34 m^2/g, 2.46 m^2/g and 2.55 m^2/g, respectively, which were larger than the initial state of 1.35 m^2/g.

In this paper, the size and distribution of micron pores before and after ultrasonic treatment were characterized by HPMI and NMR. Fig. 7a shows the changes of capillary pressure curve of the samples without ultrasonic treatment and after ultrasonic treatment for 6 h. The mercury injection curve pressure of the sample without ultrasonic treatment was always higher than that of the sample treated by ultrasonic for 6 h with the same saturation, and the median saturation pressure is reduced from 2.27 MPa to 1.54 MPa, indicating that the ultrasonic treatment increased the pore and throat radius of the sample. Since the data recorded by HPMI are pores connected to the throat and the total mercury intake and pressure of the throat, it actually characterizes the distribution of the throat. Fig. 7b is the throat radius distribution curve based on capillary pressure curve shows that the number of throats in the range of 0.1 μm-1.46 μm increased after 6 h of ultrasonic treatment, especially the average increase in the number of throats within the range of 0.61 μm-1.46 μm reached 17.9%, unfortunately, the number of throats decreased in the range of 1.82 μm to 2.2 μm. Overall, the volume of throat increased after ultrasonic treatment, which enhanced the pore-throat connectivity and the seepage capacity of the throat.

Many literatures reported that the T_2 spectrum distribution can be transformed into pore size distribution curve by combining NMR and high pressure mercury injection [48]. At present, the method commonly mentioned in literature is to use the peak value of the throat distribution curve obtained by HPMI and the T_2 spectrum distribution curve obtained by NMR to solve the conversion coefficient, and then convert the T_2 spectrum into the pore radius. However, the high pressure mercury injection curve represents the distribution of the throat only, and the T_2 spectrum is the response of all pores and throat signals in the core. Therefore, the size and distribution of pore and throat characterized by HPMI and NMR have large errors. The maximum pore radius is only 5 μm − 10 μm when the NMR T_2 spectrum is converted to pore size distribution according to the pore size distribution of high pressure mercury, which is inconsistent with the actual situation. In this paper, a new method was designed to convert the relaxation time into the pore radius. The method emphasized that the left peak of T_2 spectrum in NMR represents the throat and the right peak represents the pore. Conversion coefficient between peak value of throat distribution curve obtained by high pressure mercury injection and left peak of T_2 spectrum.

The relation between relaxation time T_2 and aperture r is expressed as [49]:

$$T_2 = \frac{1}{\rho}\frac{V}{S} = \frac{1}{\rho}\frac{r}{c} \tag{1}$$

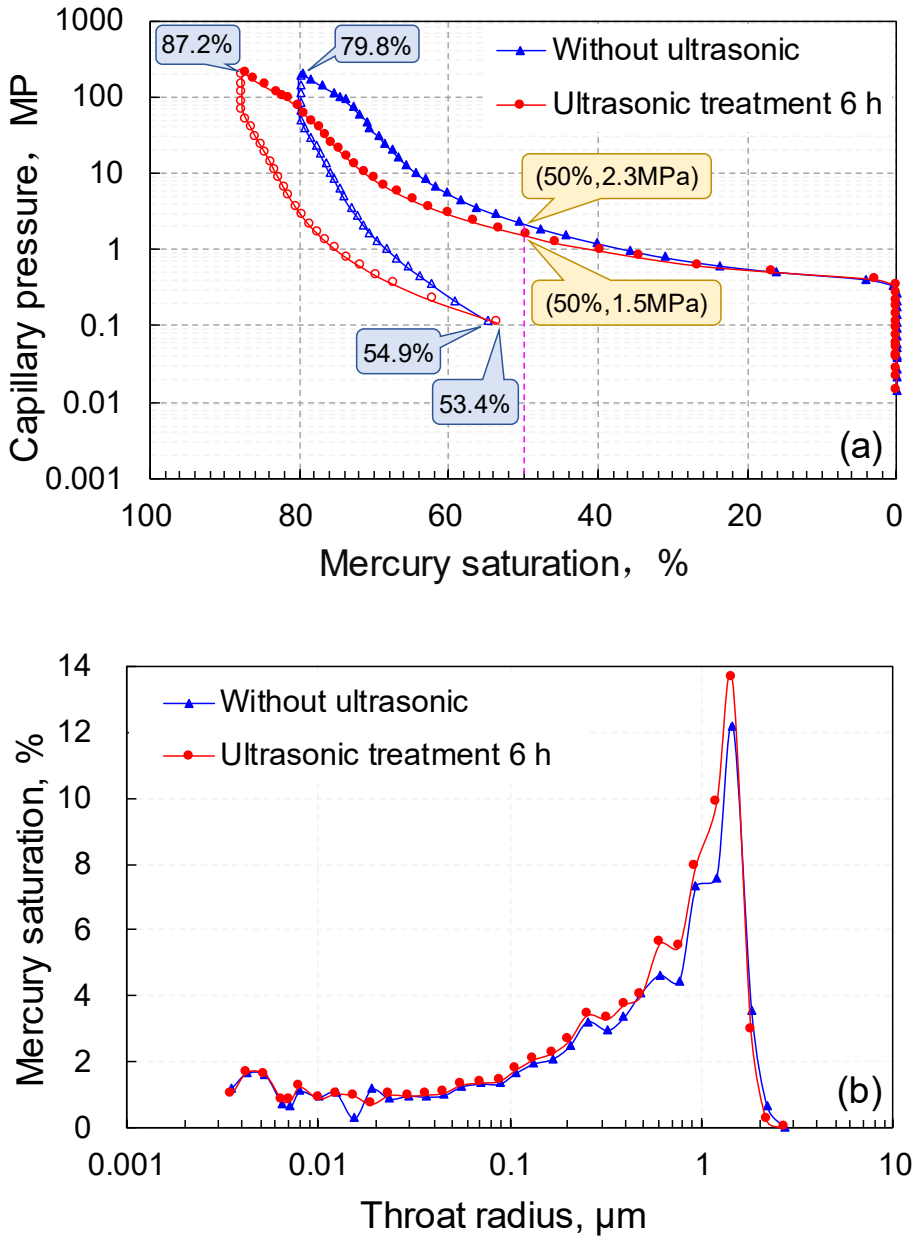

Fig. 7. The change of laryngeal size after 6 h of ultrasonic treatment (a) the change of capillary force curve (b) the size and distribution of laryngeal size.

where, ρ is the transverse surface relaxivity rate, μm/ms; c is the shape factor (in general, shape factor is 2); r is pore radius, μm; and T_2 is relaxation time, ms. Fig. 8 shows the combination of throat distribution curve without ultrasonic wave and T_2 spectrum of saturated water without ultrasonic. The T_2 value of the left peak of NMR is 7.94 ms, and the single peak of the throat distribution curve is 1.46 μm. According to Eq. (1), the ransverse surface relaxivity rate can be calculated as 0.092 μm /ms.

The T_2 spectrum can be converted to the pore size distribution curve according to the determined ransverse surface relaxivity rate. Fig. 9a shows the T_2 spectrum distribution of ultrasonic treatment at different times, and the pore size distribution curve of ultrasonic treatment at different times is obtained by converting this figure as shown in Fig. 9b. It can be seen from the figure that the number of pores increases in the range of 3 μm-32.7 μm after ultrasonic treatment, and the number of pores increases with the increase of the ultrasonic treatment time, especially after 2 h of ultrasonic treatment, nevertheless, the number of pores with radius greater than 32.7 μm decreased slightly. After ultrasonic treatment for 6 h, the minimum pore radius increased from 0.058 μm to 0.073 μm and the maximum pore radius was reduced from 92.1 μm to 73.2 μm.

In conclusion, the number of nanopores and mesopores in core increases with ultrasonic treatment, at the same time, the size of nanopores and throat increase, on the contrary, the number of macropores decreases. It is one of the reasons for the increase of core permeability and porosity.

3.3. Connectivity

It can be seen from Fig. 7a, the mercury injection saturation increased from 79.8% to 87.2% with the same maximum mercury inlet pressure after ultrasonic treatment for 6 h, and the mercury removal efficiency increases from 31.2% to 38.7%. The increase of mercury saturation and mercury removal efficiency indicated that the pore throat

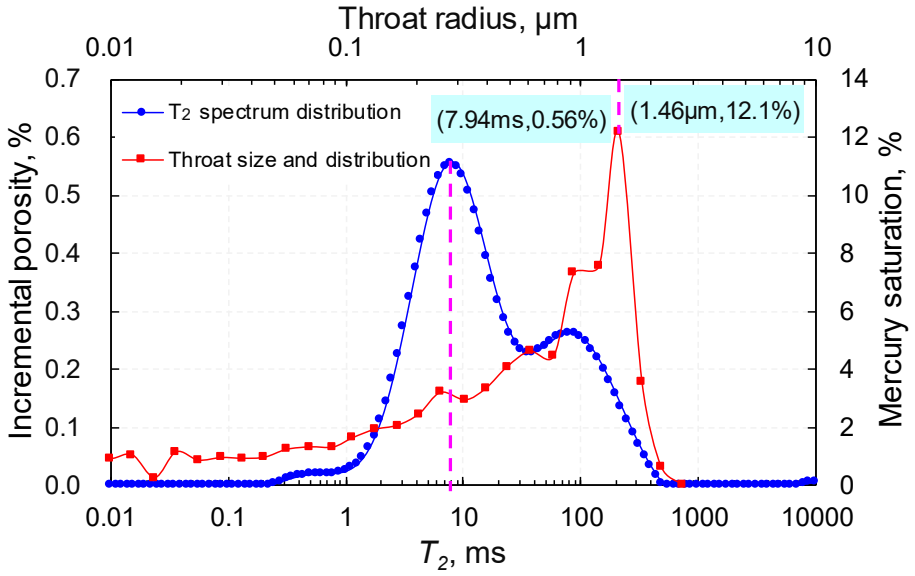

Fig. 8. Combination of throat distribution curve without ultrasonic wave and T_2 spectrum of saturated water without ultrasonic.

connectivity was improved after ultrasonic treatment. One of the reasons is that the increase of throat size in the core caused by the cavitation of the ultrasonic wave promotes the connection of pores. Another reason is that the rock is forced to vibrate under the action of high-frequency vibration of ultrasonic wave resulting in the cements dominated by clay minerals in the core to fall off the surface of the pores, thus changing the pore structure in the porous medium and connecting the pores.

Table 1 shows the results of XRD test after ultrasonic treatment for different time. It can be seen from the table that the clay minerals content in the rock is 27.7% without ultrasonic, and decreases to 17.1% after ultrasonic treatment for 2 h. The content of clay minerals in the rock after ultrasonic treatment for 4 h and 6 h is 10.8% and 7.8%, respectively. Obviously, the content of clay minerals in rock decreases with the extension of ultrasonic treatment time, on the contrary, the content of other minerals except clay minerals has increased. This does not mean that the ultrasonic action transforms the clay minerals into other minerals but the high-frequency oscillation of ultrasonic waves peels off the clay minerals in the rock led to the content of clay minerals decreases, and the content of other minerals without shedding increases relatively, the result is that the content of other minerals except clay minerals increases relatively. Fig. 10a is a microscopic view of the rock surface without ultrasonic waves, it can be seen from the figure that the particles on the rock surface are filled with cementing material. Fig. 10b shows the microscopic view of the rock surface after ultrasonic treatment for 6 h, affected by the ultrasonic high-frequency vibration and cavitation, the cemented material between the particles falls off, but a large number of rock and mineral particles remain. Inside the porous medium, the clay minerals on the surface of mesopores and micropores fall off and migrate to the macropore precipitation, resulting in the decrease of macropore size, which explains why the number of mesopores increases and the number of macropores decreases after ultrasonic treatment. In addition, it is also one of the reasons for the improvement of pore connectivity of reservoirs after ultrasonic treatment.

Combined with the conclusions in Section 3.2, it is concluded that there are two main reasons for the increase of rock permeability with the action of ultrasonic. One reason is that the clay minerals fall off from the rock surface and migrate into the large pores to sediment with the high-frequency vibration of ultrasonic waves, caused the throat size to increase, further, the originally blocked throat is dredged and the pore throat connectivity is improved. Another reason is that the continuous impact of high pressure released by cavitation on the surface caused pore and throat expansion and increases permeability.

3.4. Microscopic heterogeneity

Fractal dimension is often used to quantitatively characterize the microstructural complexity such as pore or particle size distribution, pore surface roughness and streamline curvature. The fractal dimension of the reservoir core is generally 2 to 3, the smaller the fractal dimension is, the weaker the heterogeneity is. Based on the experimental results of high pressure mercury injection, this paper analyzes the variation characteristics of microscopic heterogeneity of core after ultrasonic action from qualitative and quantitative perspectives. It can be seen from Fig. 7a that the mercury injection curve after ultrasonic treatment for 6 h is below the initial mercury inlet injection curve, the saturation with the same mercury injection pressure range is larger means that the "platform area" of the mercury injection curve is more gentle, indicating that the microscopic heterogeneity of the pore-throat was weakened after ultrasonic treatment.

According to the theory of porous media classification, the relationship between mercury volume and pore fractal characteristics is [50]:

$$S_{Hg} = 1 - \left(\frac{P_c}{P_{C,min}}\right)^{D-3} \tag{2}$$

where, S_{Hg} is the cumulative volume fraction of mercury in pores, %; P_c is capillary pressure, MPa; $P_{c,\min}$ is the minimum capillary pressure, MPa; D is fractal dimension.

Take the logarithm of both sides of Eq. (2) to obtain:

$$\mathrm{Lg}\left(1 - S_{Hg}\right) = (D-3)LgP_c - (D-3)LgP_{c,min} \tag{3}$$

The fractal dimension can be obtained by linear regression of the experimental data of HPMI using Eq. (3). The results are shown in Fig. 11, the fitting linear correlation of fractal dimension is good. The fractal dimensions of the original state and 6 h after ultrasonic treatment

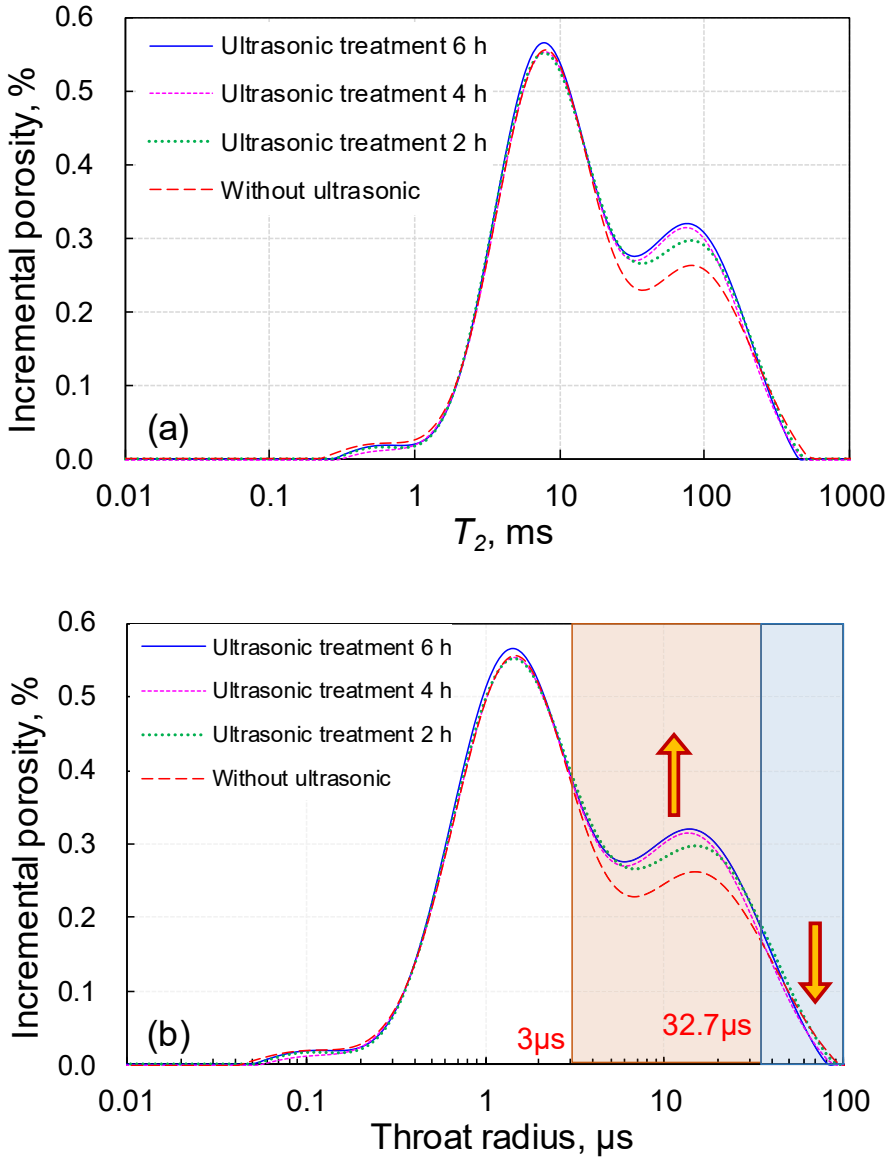

Fig. 9. Pore size changes at different time of ultrasonic treatment (a) T_2 spectrum distribution (b) pore size and distribution.

Table 1
Result of XRD.

Sample	Quartz	Potassium feldspar	Plagioclase	Caly mineral	Calcite	Anhedritite	Other
Without ultrasonic	20.3	10.2	21.5	27.7	8.6	3.8	7.9
Treatment for 2 h	21.5	13.1	26.8	17.1	9.5	4.1	7.9
Treatment for 4 h	23.7	14.3	29.1	10.8	9.1	4.2	8.8
Treatment for 6 h	23.5	14.1	32.7	7.8	8.9	4.1	8.9

were 2.55 and 2.53, respectively. By comparison, the fractal dimension of the sample after ultrasonic treatment was slightly reduced, mean that the pore-throat heterogeneity was slightly improved.

In addition to fractal dimension, pore-throat sorting coefficient (*Sp*) is also used to characterize microscopic heterogeneity in this paper. Pore-throat sorting coefficient is a standard deviation measure of pore-throat size in core, the larger the range of the capillary pressure curve platform area, the better the pore throat sorting of the core and the smaller the *Sp* value.

The calculation formula of *Sp* is:

$$S_P = \frac{(D_{84} - D_{16})}{4} + \frac{(D_{95} - D_5)}{6.6} \quad (4)$$

where, *Sp* is pore-throat sorting coefficient; D_{84} is the throat radius when the cumulative distribution frequency is 84%, μm; D_{16} the throat radius when the cumulative distribution frequency is 16%, μm; D_{95} the throat radius when the cumulative distribution frequency is 95%, μm; D_5 the throat radius when the cumulative distribution frequency is 5%, μm. The results show that the original pore throat sorting coefficient of the sample without ultrasonic waves is 0.657, and the pore throat sorting coefficient decreases to 0.614 after ultrasonic treatment for 6 h. The qualitative analysis of high-pressure mercury injection curve and the

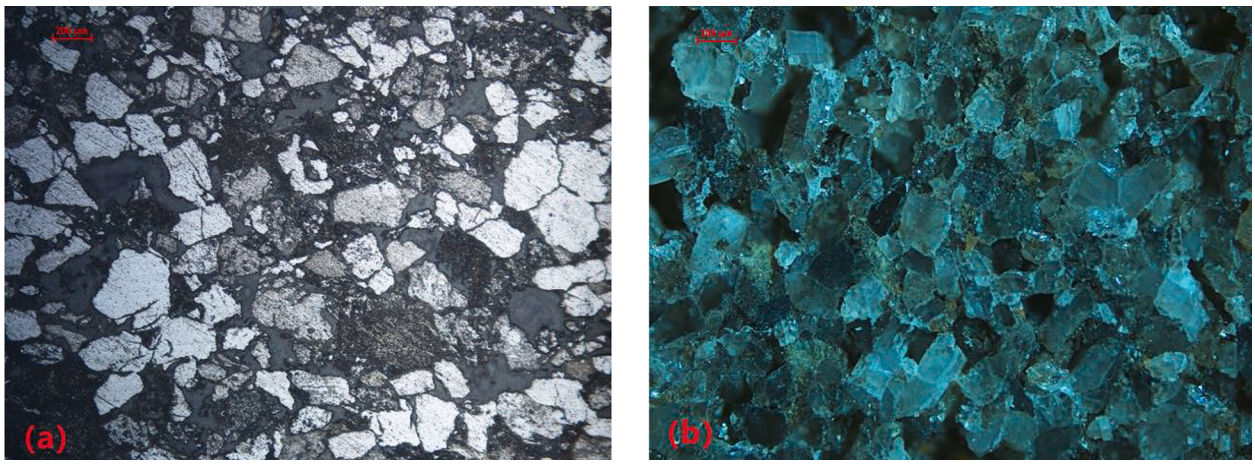

Fig. 10. Microscopic view of core surface (a) Core surface that has not been treated by ultrasound (b) Core surface treated with ultrasonic for 6 h.

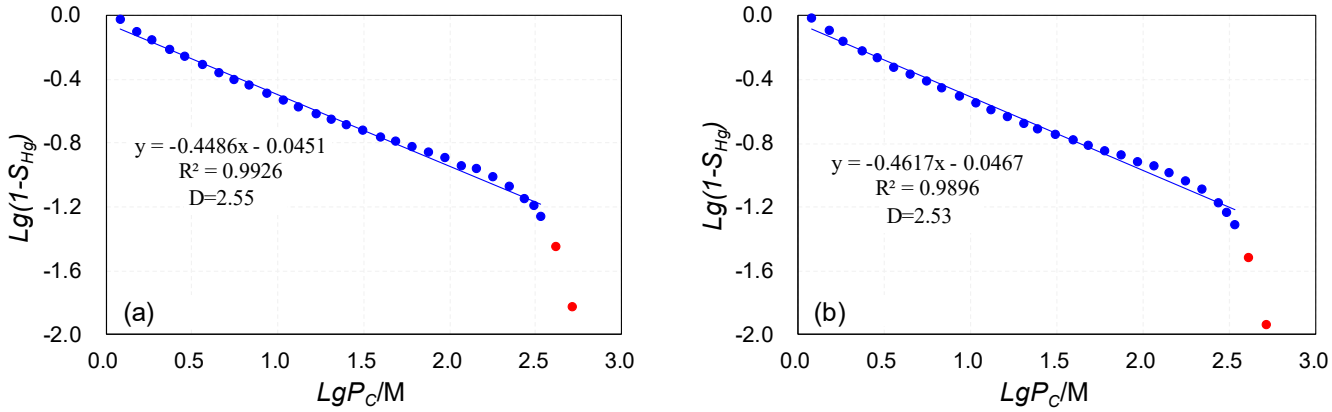

Fig. 11. Fractal Dimension Fitting (a)Without ultrasonic is 2.55 (b) ultrasonic treatment for 6 h is 2.53.

quantitative analysis of fractal dimension and pore throat sorting coefficient show that the microscopic heterogeneity of pore throat is weakened after ultrasonic treatment, which is conducive to the seepage of oil and water and thus reduces the pressure loss near the well zone.

4. Conclusion

The in-situ cores from Upper Triassic Yanchang formation of the Chang 6 sandstone reservoir in the Ordos Basin were treated by 28 kHz and 120 W ultrasonic waves for 0, 2, 4, and 6 h, with gas permeability of 4.6 mD, 10.4 mD, 11.9 mD and 12.4 mD, and porosity of 14.0%, 14.5%, 14.6% and 14.9%, respectively. Both permeability and porosity increased after ultrasonic treatment, whereas the increase of permeability was greater than that of porosity. According to the result of LTNA, the number and size of micropores increased after ultrasonic activations, and the increase was greater with the extension of treating time, without pore type changing. Capillary pressure curve shows that the number of throats in the range of 0.1 μm-1.46 μm increased after 6 h of ultrasonic treatment, the number of throats decreased in the range of 1.82 μm to 2.2 μm. Overall, the volume of throat increased after ultrasonic treatment, which enhanced the pore-throat connectivity and the fluid flow capacity in porous media. After ultrasonic treatment of 6 h, the number of pores increases in the range of 3 μm-32.7 μm, nevertheless, the number of pores with radius greater than 32.7 μm decreased slightly, the minimum pore radius increased from 58 to 73 nm and the maximum pore radius was reduced from 92.1 μm to 73.2 μm. After the same-period ultrasonic treatment, the fractal dimensions reduced to 2.53 and the pore throat sorting coefficient decreased from 0.657 to 0.614, which means the ultrasonic wave weakens the microscopic heterogeneity.

CRediT authorship contribution statement

Leng Tian: Investigation, Writing – review & editing, Project administration. **Hengli Wang:** Conceptualization, Methodology, Formal analysis, Investigation, Writing – original draft, Visualization. **Tao Wu:** Investigation, Validation. **Haien Yang:** Software. **Shuwen Xu:** Resources. **Xiaolong Chai:** Visualization, Validation. **Kaiqiang Zhang:** Conceptualization, Methodology, Supervision, Writing – review & editing.

Declaration of Competing Interest

The authors declare that they have no known competing financial interests or personal relationships that could have appeared to influence the work reported in this paper.

Acknowledgement

The authors acknowledge the financial supports from the National Natural Science Foundation of China (No. 51974329).

References

[1] Y. Wang, Q. Shang, L. Zhou, Z. Jiao, Utilizing macroscopic areal permeability heterogeneity to enhance the effect of CO_2 flooding in tight sandstone reservoirs in the Ordos Basin, J. Petrol. Sci. Eng. 196 (2021), 107633.

[2] F. Liu, M. Wang, Review of low salinity waterflooding mechanisms: wettability alteration and its impact on oil recovery, Fuel 267 (2020), 117112.

[3] H. Wang, L. Tian, X. Chai, J. Wang, K. Zhang, Effect of pore structure on recovery of CO_2 miscible flooding efficiency in low permeability reservoirs, J. Petrol. Sci. Eng. 208 (2022), 109305.

[4] D. Zhang, P.G. Ranjith, M.S.A. Perera, C.P. Zhang, Influences of test method and loading history on permeability of tight reservoir rocks, Energy. 195 (2020), 116902.

[5] H. Wang, G. Wang, Z. Chen, C.K. Wong Ron, Deformational characteristics of rock in low permeable reservoir and their effect on permeability, J. Petrol. Sci. Eng. 75 (2010) 240–243.

[6] Q. Yu, Y. Liu, X. Liu, D. Yao, Y. Yu, Experimental study on seepage flow patterns in heterogeneous low-permeability reservoirs, J. Pet. Explor. Prod. Technol. 8 (2018) 589–596.

[7] Y. Jin, K. Chen, M. Chen, N. Grapsas, Gas expansion-induced acceleration effect in high-pressure gas flows near a wellbore, J. Porous Media 15 (2012) 317–328.

[8] J.J.L. Higdon, G.P. Muldowney, Resistance functions for spherical particles, droplets and bubbles in cylindrical tubes, J. Fluid Mech. 298 (1995) 193–210.

[9] R. Czarnota, J. Stopa, D. Janiga, P. Kosowski, P. Wojnarowski Semianalytical horizontal well length optimization under pseudosteady-state conditions. Proceeding of 2018 2nd Interna-tional Conference on Smart Grid and Smart Cities (ICSGSC), August 12−14, 2018, IEEE, 2018, pp 68−72.

[10] J. Wu, Y. Liu, L. Wei, K. Wu, Q. Lin, L. Liu, J. Zhang, Scale inhibition in injection water with magnetic treatment in Xifeng Oilfield. Petroleum Exploration and Development. 2010, 37(04):490-493+507.

[11] S. Henryk, J. Włodzimierz, M.D. Mościcki, Pollution of near-surface zone in the vicinity of gas wells, Geoderma 197–198 (2013) 193–204.

[12] A.R. Ismail, A. Aftab, Z.H. Ibupoto, The novel approach for the enhancement of rheological properties of water-based drilling fluids by using multi-walled carbon nanotube, nanosilica and glass beads, J. Petrol. Sci. Eng. 139 (2016) 264–275.

[13] H. Abdul, T.K. Ari, R. Agus, Condensate gas blockage simulation in a gas reservoir: a case study of a gas field in the Mahakam Delta. East Kalimantan, Indonesia, Arabian J. Geosci. 11 (2018) 363.

[14] X. Zhang, X. Chen, L. Ma, Y. Zhou, Y. Shi, G. Yang, Research and application of ultrasonic oil production technique, Ground Water (2013,) 01–25.

[15] C. Gu, J. Yu, Ultrasonic research and application, Prod. Technol. Drill. Prod. Technol. 26 (2003) 59–66.

[16] P.M. Roberts, A. Venkitaraman, M.M. Sharma, Ultrasonic removal of organic deposits and polymer-induced formation damage, SPE 62046 (2000) 19–24.

[17] T. Hamida, T. Babadagli, Analysis of capillary interaction and oil recovery under ultrasonic waves, Transp. Porous Media 70 (2007) 231–255.

[18] O.G. Gunal, M. Islam, Alteration of asphaltic crude rheology with electromagnetic and ultrasonic irradiation, J. Pet. Sci. Eng. 26 (2000) 263–272.

[19] K. Naderi, T. Babadagli, Infuence of intensity and frequency of ultrasonic waves on capillary interaction and oil recovery from diferent rock types, Ultrason. Sonochem. 17 (3) (2010) 500–508.

[20] R. Czarnota, D. Janiga, J. Stopa, P. Wojnarowski, Acoustic investigation of CO_2 mass transfer into oil phase for vapor extraction process under reservoir conditions, Int. J. Heat Mass Transf. 127 (2018) 430–437.

[21] H. Wang, L. Tian, K. Zhang, Z. Liu, C. Huang, L. Jiang, X. Chai, How is ultrasonic-assisted CO_2 EOR to unlock oils from unconventional reservoirs? Sustainability. 13 (2021) 10010.

[22] V. Grifng, Theoretical explanation of the chemical effects of ultrasonics, J. Chem. Phys. 18 (7) (1950) 997–998.

[23] T. Hamida, T. Babadagli Immiscible displacement of oil by water in consolidated porous media due to capillary imbibition under ultrasonic waves. J. Acoust. Soc. Am. 122, 3, 1539-1555.

[24] H. Tarek, B. Tayfun Effect of Ultrasonic Waves on the Capillary Imbibition Recovery of Oil, Publisher: Society of Petroleum Engineers (SPE) Paper presented at the SPE Asia Pacific Oil and Gas Conference and Exhibition, April 5–7, 2005: SPE-92124-MS.

[25] H. Tarek, T. Babadagli Capillary interaction of different oleic and aqueous phases between matrix and fracture under ultrasonic waves. Society of Petroleum Engineers (SPE) Paper presented at the SPE Europec/EAGE Annual Conference, June 13–16, 2005. Paper Number: SPE-94105-MS.

[26] A. Mohammed, A.A.M. Mohammed, S.A. Emad, Improved oil recovery by application of sound waves to water flooding. Society of Petroleum Engineers (SPE) Paper presented at the SPE Middle East Oil and Gas Show and Conference, March 11–14, 2007. SPE-105370-MS.

[27] H.S. Siti, G. Adel, Conventional and electrical EOR review: the development trend of ultrasonic application in EOR, J. Pet. Explor. Prod. Technol. 10 (2020) 2923–2945.

[28] Z. Wang, Y. Xu, Review on application of the recent new high-power ultrasonic transducers in enhanced oil recovery field in China, Energy. 89 (2015) 259–267.

[29] Z. Wang, R. Fang, H. Guo, Advances in ultrasonic production units for enhanced oil recovery in China, Ultrason. Sonochem. 60 (2020), 104791.

[30] M.A. Muhammed, M. Mahmoud, Antenna array design for enhanced oil recovery under oil reservoir constraints with experimental validation, Energy. 66 (2016) 868–880.

[31] M.S. Mullakaev, V.O. Abramov, A.V. Abramova, Ultrasonic automated oil well complex and technology for enhancing marginal well productivity and heavy oil recovery, J. Pet. Sci. Eng. 159 (2017) 1–7.

[32] A.C.T. Aarts, G. Ooms, K.J. Bil, E.T.G. Bot, Enhancement of liquid flow through a porous medium by ultrasonic radiation, SPE J. 4 (1999) 321.

[33] V.P. Dyblenko, Wave Methods for Stimulating Oil Reservoirs with Hard-To-Extract Reserves: Review and Classification, VNIIOENG, Moscow, 2008.

[34] G. Ali, E. Mehdi, R. Masoud, F. Ali, Experimental investigation of ultrasonic treatment effectiveness on pore structure, Ultrason. Sonochem. 51 (2019) 305–314.

[35] X. Li, C. Pu, X. Chen, F. Huang, H. Zheng, Study on frequency optimization and mechanism of ultrasonic waves assisting water flooding in low-permeability reservoirs, Ultrason. Sonochem. 70 (2021), 105291.

[36] X. Li, J. Zhang, C. Wu, T. Hong, Y. Zheng, C. Li, B. Li, R. Li, Y. Wang, X. Liu, Z. Zhao, Q. Qi, X. Du, Experimental research on the effect of ultrasonic waves on the adsorption, desorption, and seepage characteristics of shale gas, ACS Omega 6 (2021) 17002–17018.

[37] Z. Tang, C. Zhai, Q. Zou, Changes to coal pores and fracture development by ultrasonic wave excitation using nuclear magnetic resonance, Fuel 186 (2016) 571–578.

[38] Q. Shi, Y. Qin, B. Zhou, Porosity changes in bituminous and anthracite coal with ultrasonic treatment, Fuel 255 (2019), 115739.

[39] P. Liu, A. Liu, F. Zhong, Pore/fracture structure and gas permeability alterations induced by ultrasound treatment in coal and its application to enhanced coalbed methane recovery, J. Petrol. Sci. Eng. 205 (2021), 108862.

[40] Y. Sun, C. Zhai, H. Ma, Changes of coal molecular and pore structure under ultrasonic stimulation, Energy Fuels 35 (2021) 9847–9859.

[41] X. Li, J. Zhang, R. Li, Q. Qi, Y. Zheng, C. Li, B. Li, C. Wu, T. Hong, Y. Wang, X. Du, Z. Zhao, X. Liu, Numerical simulation research on improvement effect of ultrasonic waves on seepage characteristics of coalbed methane reservoir, Energies 14 (2021) 4605.

[42] F. Zhao, D. Cheng, Changes in pore size distribution inside sludge under various ultrasonic conditions, Ultrason. Sonochem. 38 (2017) 390–401.

[43] Z. Zhang, X. Liu, D. Li, Y. Lei, T. Gao, B. Wu, J. Zhao, Y. Wang, G. Zhou, H. Yao, Mechanism of ultrasonic impregnation on porosity of activated carbons in non-cavitation and cavitation regimes, Ultrason. Sonochem. 51 (2019) 206–213.

[44] K.S.W. Sing, D.H. Everett, R.A.W. Haul, Reporting physisorption data for gas/solid systems with special reference to the determination of surface area and porosity, Pure Appl. Chem. 57 (4) (1985) 603–619.

[45] S. Brunaure, P.H. Emmett, E. Teller, Adsorption of gases in multimolecular layers, J. Am. Chem. Soc. 60 (2) (1938) 309–319.

[46] E.P. Barrett, L.G. Joyner, P.H. Halenda, The determination of pore volume and area distribution in porous substance. I. computations from nitrogen isotherms, J. Am. Chem. Soc. 73 (1) (1951) 373–380.

[47] J. Lai, G. Wang, Z. Wang, J. Chen, X. Pang, S. Wang, Z. Zhou, Z. He, Z. Qin, X. Fan, A review on pore structure characterization in tight sandstones, Earth Sci. Rev. 177 (2018) 436–457.

[48] F. Zhang, Z. Jiang, W. Sun, Y. Li, X. Zhang, L. Zhu, M. Wen, A multiscale comprehensive study on pore structure of tight sandstone reservoir realized by nuclear magnetic resonance, high pressure mercury injection and constant-rate mercury injection penetration test, Marine Petrol. Geol. 109 (2019) 208–222.

[49] X. Shao, X. Pang, F. Jiang, L. Li, Y. Huyan, D. Zhene, Reservoir characterization of tight sandstones using nuclear magnetic resonance and incremental pressure mercury injection experiments: implication for tight sand gas reservoir quality, Energy Fuels 31 (2017) 10420–10431.

[50] J. Liu, D. Lu, P. Li, Nano-scale dual-pore-shape structure and fractal characteristics of transitional facies shale matrix, J. Nat. Gas Sci. Eng. 68 (2019), 102907.